ANN modeling and multiobjective genetic algorithm optimization of pulsed laser welding of Ti6Al4V alloy sheets with various thicknesses

Cite as: J. Laser Appl. **33**, 012056 (2021); https://doi.org/10.2351/7.0000356
Submitted: 18 December 2020 . Accepted: 25 January 2021 . Published Online: 16 February 2021

Seyed Amin Bagherzadeh, Majid Shamsipour, Mohammad Javad Kholoud, and Mohammad Hossein Razavi Dehkordi

Journal of Laser Applications ARTICLE scitation.org/journal/jla

ANN modeling and multiobjective genetic algorithm optimization of pulsed laser welding of Ti6Al4V alloy sheets with various thicknesses

Cite as: J. Laser Appl. 33, 012056 (2021); doi: 10.2351/7.0000356
Submitted: 18 December 2020 · Accepted: 25 January 2021 ·
Published Online: 16 February 2021

Seyed Amin Bagherzadeh, Majid Shamsipour, Mohammad Javad Kholoud, and Mohammad Hossein Razavi Dehkordi[a)]

AFFILIATIONS

Department of Mechanical Engineering, Najafabad Branch, Islamic Azad University, Najafabad, Iran

[a)]**Author to whom correspondence should be addressed; electronic mail:** mohammadhossainrazavi@gmail.com.
Telephone: +989122435649

ABSTRACT

According to the high cost and time-consuming nature of laser welding experiments, repetition of one experiment in a wide range of data is not feasible; so, achieving unexperimented data can be interesting. Hence, the high precision predictability of artificial neural networks (ANN) seems useful. ANN is an intelligent approach to solve different problems. In this study, the experimental data belonging to the pulsed laser welding of two Ti6Al4V sheets, one of them with 1 mm thickness and the other with 1, 1.5, and 3 mm thicknesses, were used to predict the dimensions of the heat-affected zone (HAZ) and the maximum temperature. Moreover, 12 learning methods of a backpropagation network was utilized to select the best one. The Levenberg–Marquardt method had the best performance by considering the mean square error. According to the ANN results, when the laser focus is at the vicinity of workpiece's surface, the maximum temperature and HAZ width are achieved. It should be also mentioned that increasing thickness and welding speed results in decreasing width of HAZ. By comparing the ANN and experimental results, the maximum relative error for the temperature and HAZ width was obtained equal to 8.62% and 8.22%, respectively. Therefore, ANN can be employed as a tool to develop experimental results and predict indeterminate values in unexperimented ranges with very high precision. Furthermore, in order to optimize the parameters of laser welding, the multiobjective genetic algorithm was used to reduce the HAZ width. The genetic algorithm specified that the HAZ width can be reduced to 0.24 mm by increasing the velocity and thickness.

Key words: laser welding, artificial neural network (ANN), genetic algorithm (GA), Ti6Al4V alloy, heat affected zone (HAZ), different thicknesses

I. INTRODUCTION

Laser discovery has been led to a massive evolution in newfangled industries. In laser welding, high energy density laser beam is absorbed on the metal surface and causes melt formation. Laser welding is extensively utilized to join different pieces to each other because of its speed, quality, high aspect ratio, and small heat-affected zone (HAZ). The prediction and determination of molten pool dimensions, HAZ, and the temperature field have a key role in mechanical characteristics and joint quality in both pulsed and continuous laser welding applications.[1–5] Weld quality is mostly evaluated by weld bead geometry, mechanical characteristics, distortion, and HAZ. Due to low density, appropriate mechanical properties at high temperatures, and good corrosion resistance, titanium and titanium alloys have had a successful performance in a wide range of applications including medical, aerospace, and automobile and petrochemical industries.[6] Besides, titanium alloys can be considered as a suitable substitution for aluminum when the working temperature exceeds 130 °C.[7]

Given that localized heating together with rapid cooling in laser welding result in creating residual stresses in the workpiece main structure and weld zone, hence, the existence of them can lead to

making harmful effects like corrosion cracks, hydrogen crack, and fatigue resistance drop. In order to reduce the aforementioned harmful effects, it is required to investigate the parameters-affected temperature field and HAZ dimensions. Wide-ranging experimental studies have been carried out in the field of laser welding. For instance, Berretta *et al.*[8] investigated the effect of changing the position of the laser beam on some weld properties like weld geometry, penetration depth, and sensitivity to crack as well as mechanical properties such as tensile strength and microhardness. They used a 3000 W peak power Nd:YAG laser welding to join 420 and 304 stainless steel samples having 0.8 mm thickness and 50 mm length. Their variable parameter was the displacement of the laser beam in the range of 0.1–0.2 mm with respect to the interface of the two base metals. Cao and Jahazi[9] performed the joint of two sheets of Ti6Al4V alloy using Nd:YAG laser welding. They scrutinized the effect of welding speed on the microstructure and mechanical properties of workpieces. The acquired weld zone mainly included α martensite phase which resulted in a 20% increase in hardness compared to the base metal. It should be also mentioned that the heat-affected zone included a combination of two α martensite and α primary phases. Furthermore, Taban *et al.*[10] performed extensive investigations on the corrosion, toughness, fatigue, strength, and microhardness of corrosion-resistant steel having 12% chromium. They concluded that increasing grain size in HAZ leads to a sensible decrease in microhardness. In addition, Aleksander[11] welded 2 mm thickness Ti6Al4V sheets in the butt weld configuration using disk laser technology and argon shielding gas and studied the effect of laser parameters on weld quality. Their measurement criteria for the weld quality were bending and tensile tests and microhardness. Torkamany *et al.*[12] also examined the joint of two dissimilar metals, i.e., Ti6Al4V and niobium (Nb), by means of a 1.5 kW peak power Nd:YAG laser. According to the different properties of these two metals, especially melting temperature, specific heat capacity, and heat transfer coefficient, the created molten pool was 12 times bigger in Ti6Al4V compared to niobium. By locating the laser beam on the titanium piece relative to the joint position, it was observed that keyhole and conduction mode welding create in titanium and niobium, respectively. Moreover, Caiazzo *et al.*[13] investigated the optimization of welding parameters using the experimental results of Ti6Al4V laser welding. Welding speed, laser power, and focal position were considered as input parameters. They realized changing the focal position has an impressive effect on the HAZ width and fusion zone width. Campanelli *et al.*[14] analyzed the tensile strength and microhardness of the molten pool and HAZ in a 2 mm thick Ti6Al4V sheet using fiber laser welding. Their results indicated that the molten pool and HAZ become cone-shaped through increasing welding speed. Moreover, the tensile strength of the welded workpiece was about 80% of the base metal. Ahn *et al.*[15] studied the effect of laser power, welding speed, and focal position on the molten pool shape and mechanical properties of the Ti6Al4V sheet during the process of fiber laser welding. Palanivel *et al.*[16] also analyzed the microstructure and mechanical properties of a 60 mm diameter Ti6Al4V tube using Nd:YAG laser welding. It was observed that the molten zone hardness is higher in comparison with the base metal. Ai *et al.*[17] investigated how to move the molten metal and form a keyhole in S.S 316L by a numerical and experimental study. They scrutinized the features of keyhole and behavior of melt movement during high power and penetration fiber laser welding. Additionally, they found that the biggest factor leading to melt movement and keeping the keyhole width open is the metal vapor-induced pressure. It is worthy to note that the surface tension force extremely tends to diminish the width of the keyhole. Kumar and Sinha[18] studied the mechanical properties and the microstructure of Ti6Al4V sheet in the pulsed Nd:YAG laser welding and reported the effect of heat input on the dimensions of the molten pool and HAZ. It was observed that the microhardness of the melt zone is more than that of the heat-affected zone because of α martensite phase. They also found that the tensile strength increases to the heat input of 49.98 J/mm and then decreases. Raja Kumar *et al.*[19] investigated the melt zone and vapor created in two dissimilar metals of pure titanium and Aluminum A5754 during the process of Nd:YAG laser welding. They examined the effect of changing the distance of weld line from the joint position of two workpieces on the created molten pool and vapor. The results for the mode in which the weld line was located in the joint position were an indication of making an unstable keyhole in the aluminum sample. Moreover, it was realized when the weld line is located in the titanium sample, a stable keyhole is made and the vapor temperature is obtained in the range of 5000–6000 K. Benyounis *et al.*[20] performed wide investigations in the laser welding process optimization. They utilized a CO_2 laser to join medium carbon steel and adjusted several parameters like laser power, speed, and focal position in order to achieve optimal conditions. The output values including heat input, penetration depth, and molten pool and HAZ width were considered. Moreover, they tried to reduce the costs through the correct regulation of aforementioned parameters using defining an expenditure function.

Since empirical experiments to investigate the effect of different parameters on the weld geometry and the melt zone are time-consuming and very expensive, using artificial neural network (ANN), which has been at the center of interest in recent years, is a suitable alternative for the experiments to predict the parameters of laser welding. Chang *et al.*[21] predicted the weld geometry of 304 stainless steel in the pulsed Nd:YAG laser welding through three approaches of empirical, finite element, and ANN. Pulse energy, pulse duration, and sheet thickness were considered as the variable parameters in the numerical simulation and experimental approach. The thickness of the metal sheet and the distance between two sheets were chosen as the input variables of the back-propagation algorithm in ANN, while the dimensions of weld geometry were considered as its out variable. The results showed that using the finite element method to anticipate weld dimensions in the laser welding of two sheets with a specified gap may be limited. On the other hand, a good estimation of weld geometry can be acquired using ANN. Similarly, Anawa and Olabi[22] studied the laser welding of austenitic and ferritic dissimilar steels. They designed and optimized experiments using the Taguchi method and concluded that increasing laser power and welding speed leads to heightening and diminishing tensile strength, respectively. Park and Rhee[23] examined the effect of laser welding parameters (power, welding speed, and the feeding rate of filler wire) on the joint aluminum alloy. The experiments showed that the tensile strength of the weld in a specific condition is higher than the base metal. By considering weldability and efficiency, an appropriateness performance was executed to optimize the process parameters. The

genetic algorithm was employed to optimize laser power, welding speed, and the feeding rate of filler. Furthermore, they obtained the optimal value of input parameters in terms of weldability and efficiency. Besides, Sathiya *et al.*[24] utilized ANN to anticipate several parameters such as penetration depth, bead width, and tensile strength under the effect of laser welding input parameters including focal position, power, and laser head movement speed in the welding of austenitic stainless steel AISI 904L. In order to achieve optimal weld geometry having high tensile strength, they also used the genetic algorithm to study the effect of three different shielding gases (Ar, He, and N_2). The output results of optimal parameters obtained from the genetic algorithm were in a good agreement with the experimental ones. Additionally, Ismail *et al.*[25] predicted weld geometry under the influence of different parameters in the 304 stainless steel laser welding using ANN. They utilized the backpropagation algorithm to achieve the weld parameters; also, the Levenberg–Marquardt method was employed to train the network. The accuracy of the ANN model was investigated by comparing the output and experimental data. Akbari *et al.*[26] also used ANN to anticipate weld geometry and maximum temperature in the laser welding of the Ti6Al4V sheet. In order to exactly predict the parameters of laser welding, two feedforward networks having 11 and 14 neurons were utilized. The proposed ANN models with mean square errors (MSEs) of 0.079 and 0.063 resulted in the precise prediction of weld parameters. Moreover, Bagchi *et al.*[27] used the Taguchi method and ANN to optimize and predict the pulsed Nd:YAG laser welding parameters of the Hastelloy C-276 sheet. They found that the maximum depth-to-width ratio is obtained at the welding speed of 450 mm/min, pulse energy of 10 J, and frequency of 20 Hz. Kannan *et al.*[28] used the Nd:YAG laser to weld a 1 mm thick NiTinol sheet. They employed four ANN learning algorithms consisting of batch backpropagation, quick propagation, incremental backpropagation, and Legvenberg–Marquardt backpropagation to prognosticate hardness, corrosion, and weld geometry. In addition, the parameters of shielding gas nozzle distance from the weld line, laser head movement speed, focal position, and power were considered as the input parameters of ANN. Based on the mean square error, they realized that the Legvenberg–Marquardt model is the best learning algorithm. A genetic algorithm was considered to optimize the welding parameters as well. Furthermore, Sivagurumanikandan *et al.*[29] predicted and optimized several parameters including welding speed, focal position, frequency, and laser power of Nd:YAG in the joint of steel superalloy. They used the response surface method and artificial neural network (ANN) to anticipate and optimize the aforementioned parameters. The results showed that the maximum tensile strength is obtained at the welding speed of 136 mm/min, focal position of 0 mm, frequency of 13 Hz, and power of 550 W. Mehrpouya *et al.*[30] also prognosticated the thermal behavior initiated from the laser welding process of NiTi alloys. Therefore, a numerical method was employed to estimate the optimal parameters of laser welding. The results of the finite element model comparing to the experimental ones, which include transient temperature, HAZ dimensions, and fusion zones, showed a good accuracy. Moreover, ANN was employed as a tool for making a relation between the inputs and outputs of the welding process in order to find the optimal parameters of the laser. Eventually, they reported decreasing fusion zones and increasing weld quality. In order to optimize the laser welding process, Liu *et al.*[31] used the 16-group Taguchi approach together with the artificial neural network and the genetic algorithm to acquire the optimal parameters of laser beam welding concerning 316L austenitic stainless steel. The x-ray results were considered as a foundation to evaluate the porosity and quality of the weld.

In the current research, the results of experimental work conducted by Li *et al.*[32] who experimentally and numerically investigated the pulsed laser welding of two different thickness sheets of Ti6Al4V were utilized. Under the influence of various laser parameters like focal position, laser welding speed, and power, they analyzed the temperature distribution around the molten pool and also the depth and width of the molten pool and HAZ dimensions. The main goal of this research work is to predict HAZ dimensions and maximum temperature at a 2 mm distance from the weld line using ANN in the case of unexperimented data in the research conducted by Li *et al.*[32] Moreover, in addition to predict the effect of input parameters like welding speed, nozzle distance, and thickness on the HAZ dimensions and temperature, the genetic algorithm was employed to achieve the optimal parameters in order to decrease the heat affected zone.

II. EXPERIMENTAL PROCEDURE

Li *et al.*[32] used the Nd:YAG pulsed laser (IQL-20) in order to join two 60×15 mm^2 Ti6Al4V sheets, one of which has different thicknesses including 1, 1.5, and 3 mm and the other has a constant thickness of 1 mm. Argon gas was utilized to prevent the oxidation of the molten pool. The flow rate of shielding gas was equal to 15 l/min. Table I shows the chemical composition of the Ti6Al4V alloy.

According to that the melting temperature of titanium is 1650 °C and the temperature range of considered thermocouple is from 40 to 1230 °C, hence, the temperature was measured at a 2 mm distance from the weld line. It should be mentioned that two welded pieces have different thicknesses and thermal fields. To increase the precision, two thermocouples were installed on each metallic piece to register the temperature changes. The considered thermocouple is a flexible K-type thermocouple having 10 cm length, 1 mm tip diameter, and ±1% accuracy.[32] Figure 1 shows a schematic of the location of thermocouples and sheet joint.

Li *et al.* obtained the temperature values using Advantech USB 4718 module. Olympus SZ-X16 stereoscopy microscope was

TABLE I. Chemical composition of Ti6Al4 V alloy (Ref. 32).

Ti%	Al%	V%	Cu%	Mn%	Fe%	Cr%	Mo%	Si%	Sn%	Zr%	Nb%
Base	6.5	4.0	<0.02	0.02	0.04	<0.01	<0.03	0.03	<0.05	0.02	0.02

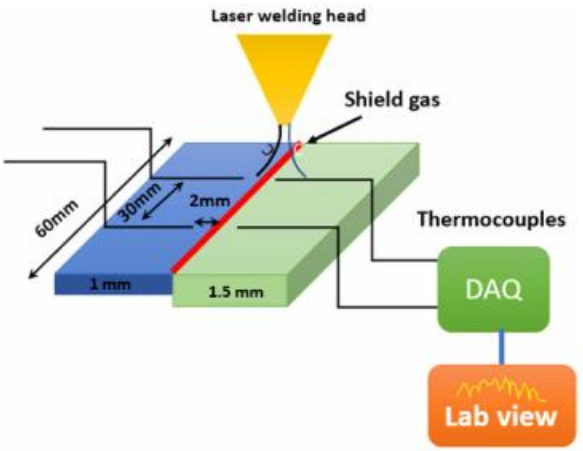

FIG. 1. A schematic of the position of thermocouples and piece dimensions.

also employed to measure molten pool dimensions and HAZ width. Some of the experimental results obtained from Ref. 32 and other data were gained through additional experiments performed by author's group that is presented in Table II. The results shown in Table II indicate concerning HAZ width and maximum measured temperature in the piece having various thicknesses based on 27 different input parameters with 180 W power, 6 ms pulse width, and 20 Hz frequency. The focal point is the distance between the laser beam focus point and the surface of the workpiece. The beam diameter at the focal point is determined by a special paper target by adjusting the distance from the bottom of the nozzle. Therefore, the smallest pierce at determined height can present the focal point position. By measuring the specific distance from the bottom of the nozzle height, the focal point is determined, and by adjusting the nozzle distance, the position of the focal point changes.

III. ARTIFICIAL NEURAL NETWORK

ANN is one of the mathematical modeling methods which is capable to achieve logical functions and make a relation between any series of related or unrelated data using the calculation and analysis speed of computer. ANN is extensively utilized in the field of prediction and modeling of various processes and has a great capability to analyze sophisticated multidimensional problems. In the current study, a backpropagation network, which is belonging to the category of feedforward networks, was used to predict the created maximum temperature and HAZ width in a different thicknesses sheet. The way it works is that the input data are processed in advance and the processing path does not return to the neurons

TABLE II. Experimental results.

Experiment No.	Welding speed (mm/s)	Thickness (mm)	Nozzle distance (mm)	Max. temperature (°C)	HAZ width (mm)
1	2	1	2	231.2	0.65
2	2	1	3	280.1	0.86
3	2	1	4	216.7	0.62
4	2	1.5	2	187.01	0.58
5	2	1.5	3	224.3	0.79
6	2	1.5	4	177.77	0.56
7	2	3	2	74.38	0.52
8	2	3	3	132.1	0.57
9	2	3	4	99.88	0.5
10	4.3	1	2	112.06	0.57
11	4.3	1	3	147.18	0.75
12	4.3	1	4	105.2	0.54
13	4.3	1.5	2	99.48	0.54
14	4.3	1.5	3	137.4	0.7
15	4.3	1.5	4	83.62	0.51
16	4.3	3	2	61.9	0.4
17	4.3	3	3	118.7	0.42
18	4.3	3	4	76.5	0.37
19	6.2	1	2	82.3	0.48
20	6.2	1	3	98.24	0.59
21	6.2	1	4	76.7	0.44
22	6.2	1.5	2	68.9	0.42
23	6.2	1.5	3	83.1	0.48
24	6.2	1.5	4	61.35	0.37
25	6.2	3	2	49.3	0.27
26	6.2	3	3	70.1	0.31
27	6.2	3	4	55.2	0.24

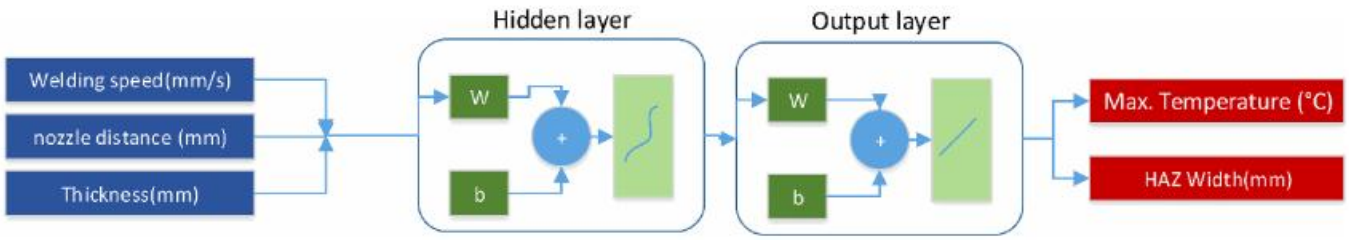

FIG. 2. The architecture of artificial neural network (ANN).

of the previous layer, and the output of each layer will only influence the next one. The learning process in ANN is such a way that this network can improve its behavior in order to achieve a specific goal just by observing its own performance in each epoch. Improvement in learning over time should be evaluated and established upon a criterion. Here, criterion means closing to the goal. In the current model, a multilayer feedforward network in which the first and second layers were considered as the input (hidden) layer having the desired number of neurons and the output one, respectively, was utilized. Figure 2 illustrates the architecture of the network in which the transfer functions of "tansig" and "pure line" were used in the hidden and last layer in that order.

According to Fig. 2, three parameters of welding speed, nozzle distance, and thickness were considered as the inputs of ANN. Moreover, temperature and HAZ width are the outputs of the network in a different thicknesses piece. In this study, the laser nozzle distance was considered the distance between the laser beam output to the workpiece surface. Hence, the 3 mm nozzle distance means locating the focus on the piece surface. Figure 3 displays an outlook of the nozzle distance.

According to Table III, 12 different algorithms were considered to train ANN. The MSE was employed to investigate and test the validation of different training methods. Equation (1) shows how to obtain the MSE,

$$\mathrm{MSE} = \frac{\sum (\text{Target-Output})^2}{n}, \tag{1}$$

where "Target" denotes real outputs, "Output" is the output resulted from the network, and "n" is the number of data.

The comparison of different types of training methods is shown in Fig. 4. It is worthy to note that the training performance of various algorithms was compared based on MSE. Every single training algorithm was compared to each other in 50 iterations with 9 neurons in the hidden layer. The minimum error is presented in different trainings.

In Fig. 4, it is shown that the Levenberg–Marquardt algorithm was chosen to train ANN because of quick convergence and small MSE. The backpropagation algorithms change network weights and bias values in such a way that the performance function declines more quickly. In the Levenberg–Marquardt, similar to semi-Newton methods, it is tried to reduce the volume of calculations by means of not calculating the Hessian matrix. When the

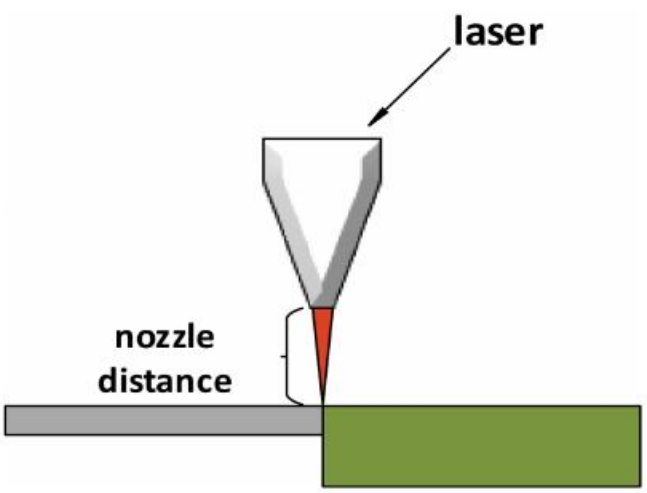

FIG. 3. An outlook of the nozzle distance.

TABLE III. Used training algorithms and their abbreviation.

Abbreviation	Algorithm
lm	Levenberg–Marquardt backpropagation
oss	One-step secant backpropagation
scg	Scaled conjugate gradient backpropagation
bfg	BFGS quasi-Newton backpropagation
cgp	Conjugate gradient backpropagation with Polak–Ribiére updates
cgb	Conjugate gradient backpropagation with Powell–Beale restarts
cgf	Conjugate gradient backpropagation with Fletcher–Reeves updates
rp	Resilient backpropagation
gdx	Gradient descent with momentum and adaptive learning rate backpropagation
gd	Gradient descent backpropagation
gdm	Gradient descent with momentum backpropagation
gda	Gradient descent with adaptive learning rate backpropagation

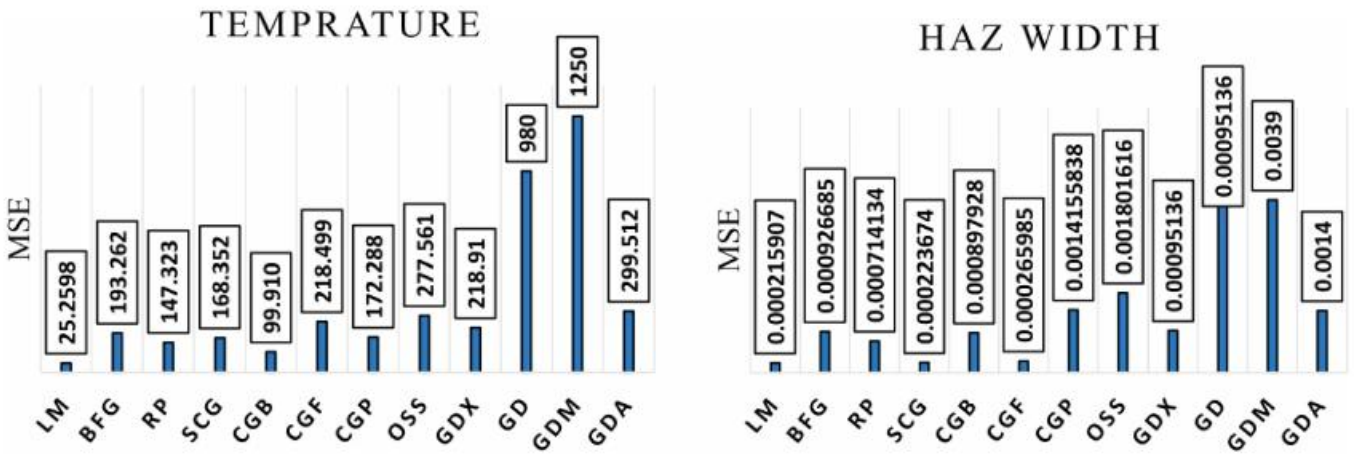

FIG. 4. The comparison of different types of artificial neural network training methods for temperature and HAZ width.

performance function is in the form of sum-of-squares (SOS), the Hessian matrix is calculated as follows:

$$H = J^T J. \tag{2}$$

Furthermore, the gradient is obtained from the following equation:

$$g = J^T e, \tag{3}$$

where J is the Jacobian matrix that includes first derivatives of network errors with respect to weights and bias and e is the vector of error networks. The Jacobian matrix is calculable through standard techniques, and the complexity of its calculations is very lower than the Hessian matrix. The Levenberg–Marquardt algorithm uses Eq. (4) approximation to calculate the Hessian matrix,

$$X_{k+1} = X_k - [J^T J + \mu I]^{-1} J^T e. \tag{4}$$

When the numerical value of μ is equal to zero, this function is converted to the Newton method to approximate the Hessian matrix. While Eq. (4) can be converted to the gradient descent method when μ is large. Therefore, μ decreases after each successful step.[33,34] Figure 5 indicates a comparison about the number of neurons available in the hidden layer in the Levenberg–Marquardt algorithm. As can be seen, the minimum MSE for HAZ width and temperature at 30 iterations is related to the network with 11 and 8 neurons in the hidden layer, respectively.

In ANN modeling, the used data are divided into two categories. One of these categories named training data is involved in the network training procedure and the other named test and validation data is employed to study the training performance of the network.

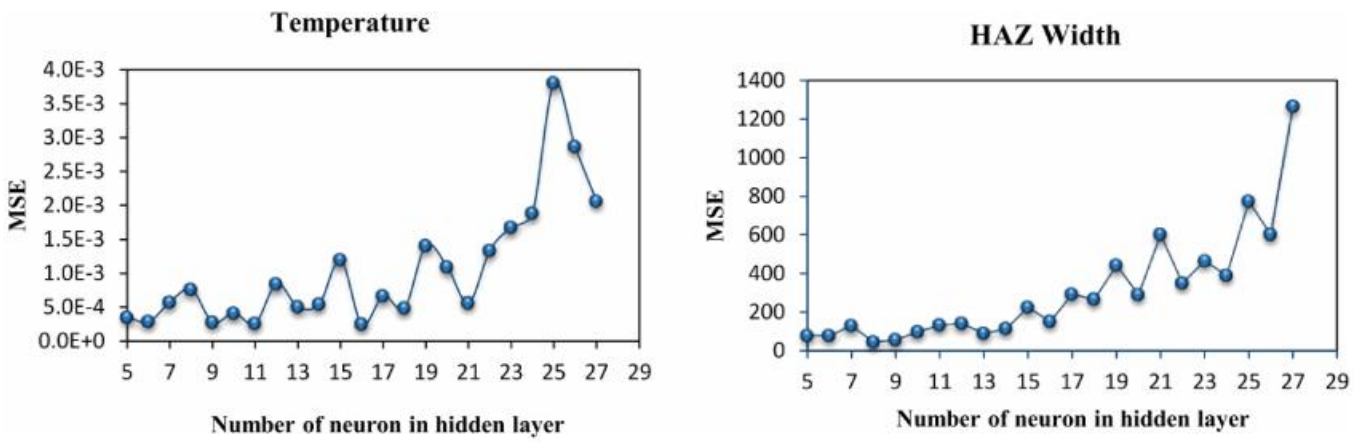

FIG. 5. The comparison of the neuron number in the hidden layer based on minimum MSE for temperature and HAZ width.

After the training procedure, the test data are applied to the network so that it does not experience them during the procedure.

Figure 6 shows the training performance in each epoch for the data related to the training, test, and validation based on MSE. According to Fig. 6, the minimum MSEs for the validation data concerning temperature and HAZ width were obtained in epoch 8 and 6, respectively. The acquired MSEs for the temperature and HAZ width are equal to 16.5078 and 0.000 103 8, respectively.

The regression graphs of temperature and HAZ width are illustrated in Figs. 7 and 8, correspondingly. As can be seen, the horizontal axis is the goal data and the perpendicular one is the ANN outputs. The best scenario occurs when the output is equal to the target, i.e., the output data from ANN and the real ones are coincident. The phrases "Fit" and R indicate the best passing line from the data and the ANN performance, respectively. According to the indicated regression graphs, 19 data (i.e., 70%) for the network training and 8 one for the validation and test (i.e., 30%) were considered. As shown in Fig. 7(a), it can be realized that the Levenberg–Marquardt algorithm shows high performance in the training stage and is precisely equal to the goal data. In comparison with Figs. 7(a) and 7(b), Fig. 7(c) indicates the maximum temperature difference in the validation data obtained from ANN. Figure 7(d) illustrates the comparison of the entire goal data with the outputs resulted from the network. Figure 8 also shows the performance of the Levenberg–Marquardt algorithm related to the HAZ width data training. Based on Figs. 8(a) and 8(b), the network in the allocated validation and training data has a better performance compared to Fig. 8(c).

Figure 9 indicates the difference between the goal data and the outputs resulted from the trained network. As can be seen, the ANN results have acceptable precision, and the model outputs and targets are almost identical. This indicates that the output value is close to the target, i.e., the network has been well trained. According to Figs. 9(a) and 9(b), the maximum difference of the target and output data in temperature and HAZ width are equal to 10.93 and 0.029, respectively. The low error values designate the very good power of network generalization to estimate the values of temperature and HAZ width which are not included in the network training set. Based on these values, it can be predicted that the network is capable to employ with a very low error in order to estimate the aforementioned values.

Figure 10 shows the relative error values of the trained data with respect to the target data based on Eq. (5). According to this figure, the maximum relative errors regarding temperature and HAZ width are equal to 8.62% and 8.22%, respectively. Hence, it can be found that the ANN output data have a little difference with the target one.

In addition, using Eq. (6), the value of R^2 error is calculated for the Levenberg–Marquardt method to evaluate the quality of the trained network. The obtained values of R^2 error for temperature and HAZ width are 0.9962 and 0.9912, respectively, which indicate a small difference in the obtained data from the trained network compared to the experimental results. Hence, due to the low obtained error, it can be concluded that the network can be generalized to untrained data,

$$\text{Relative error} = \frac{|\hat{y}_i - y_i|}{y_i} \times 100, \tag{5}$$

$$R^2 \text{ error} = 1 - \frac{\sum (y_i - \hat{y}_i)^2}{\sum (y_i - \bar{y})^2}. \tag{6}$$

In Eq. (6), y_i is the experimental data used for ANN training, $\hat{y}i$ is the data extracted from the trained network, and $\bar{y}$ is the mean value of the experimental data.

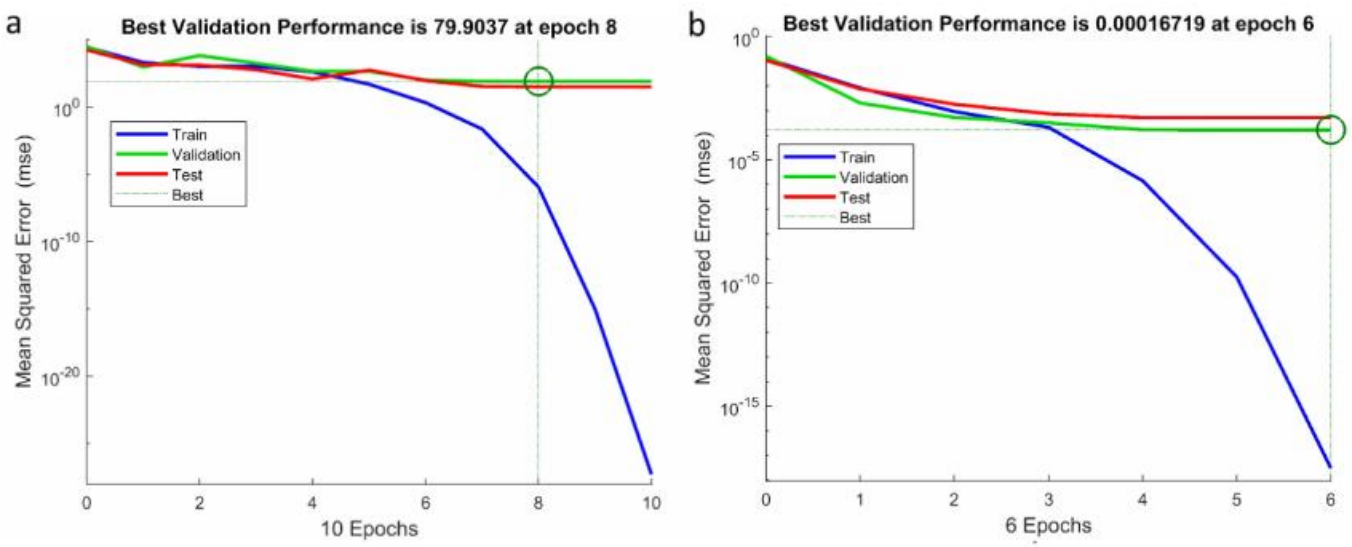

FIG. 6. The Levenberg–Marquardt training performance: (a) Temperature and (b) HAZ width.

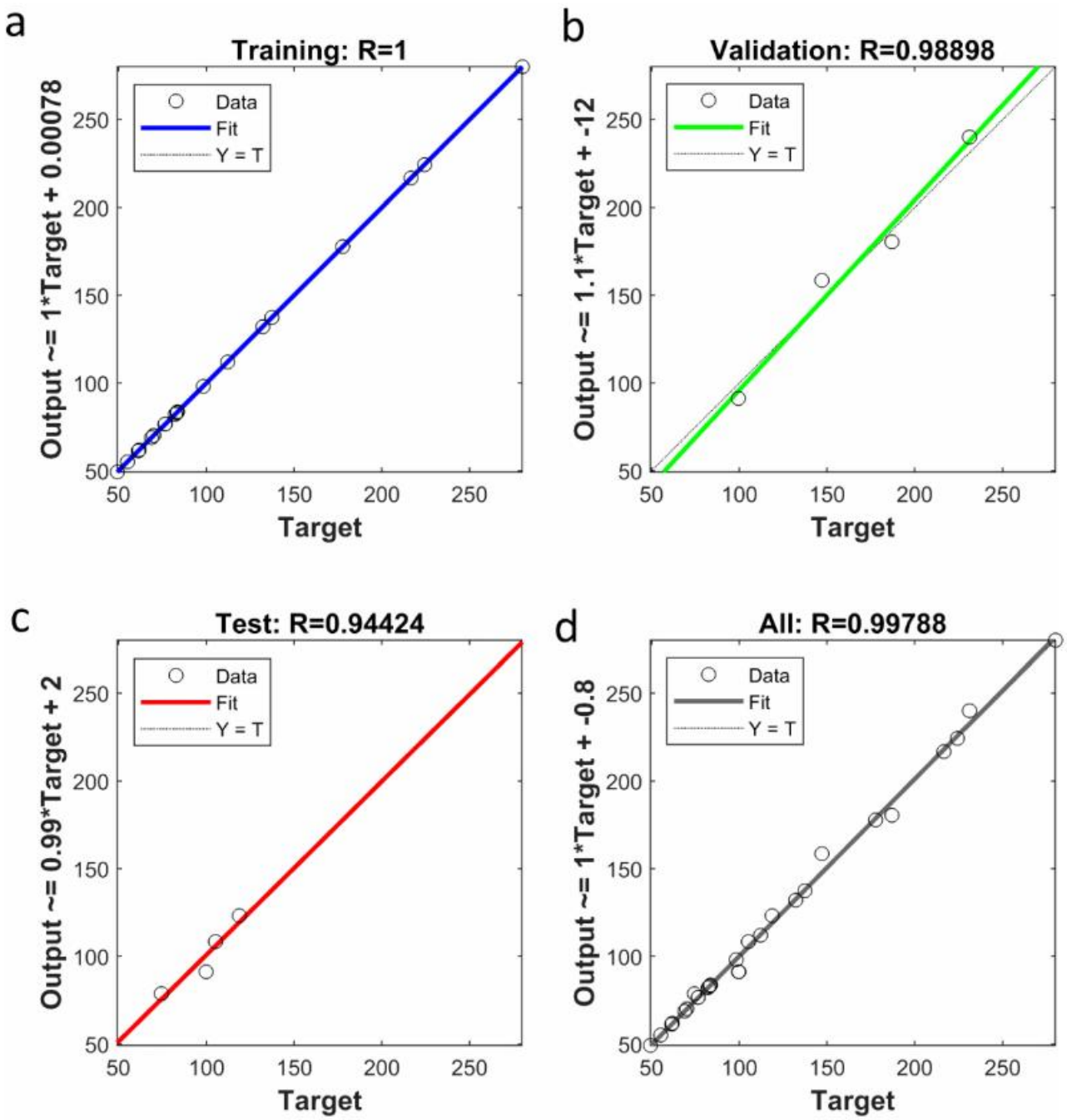

FIG. 7. Temperature regression graphs: (a) Training dataset, (b) validation dataset, (c) test dataset, and (d) all dataset.

IV. OPTIMIZATION

Optimization is a tool that allows users in research and industrial projects to find the appropriate conditions to get the answers they want. Today, this is increasingly utilized in welding owing to its complexity. The optimization procedure is shown in Fig. 11 using the genetic algorithm. The genetic algorithm consists of three main parts of selection, crossover, and mutation. According to Fig. 11, the genetic algorithm begins with a primary set of random

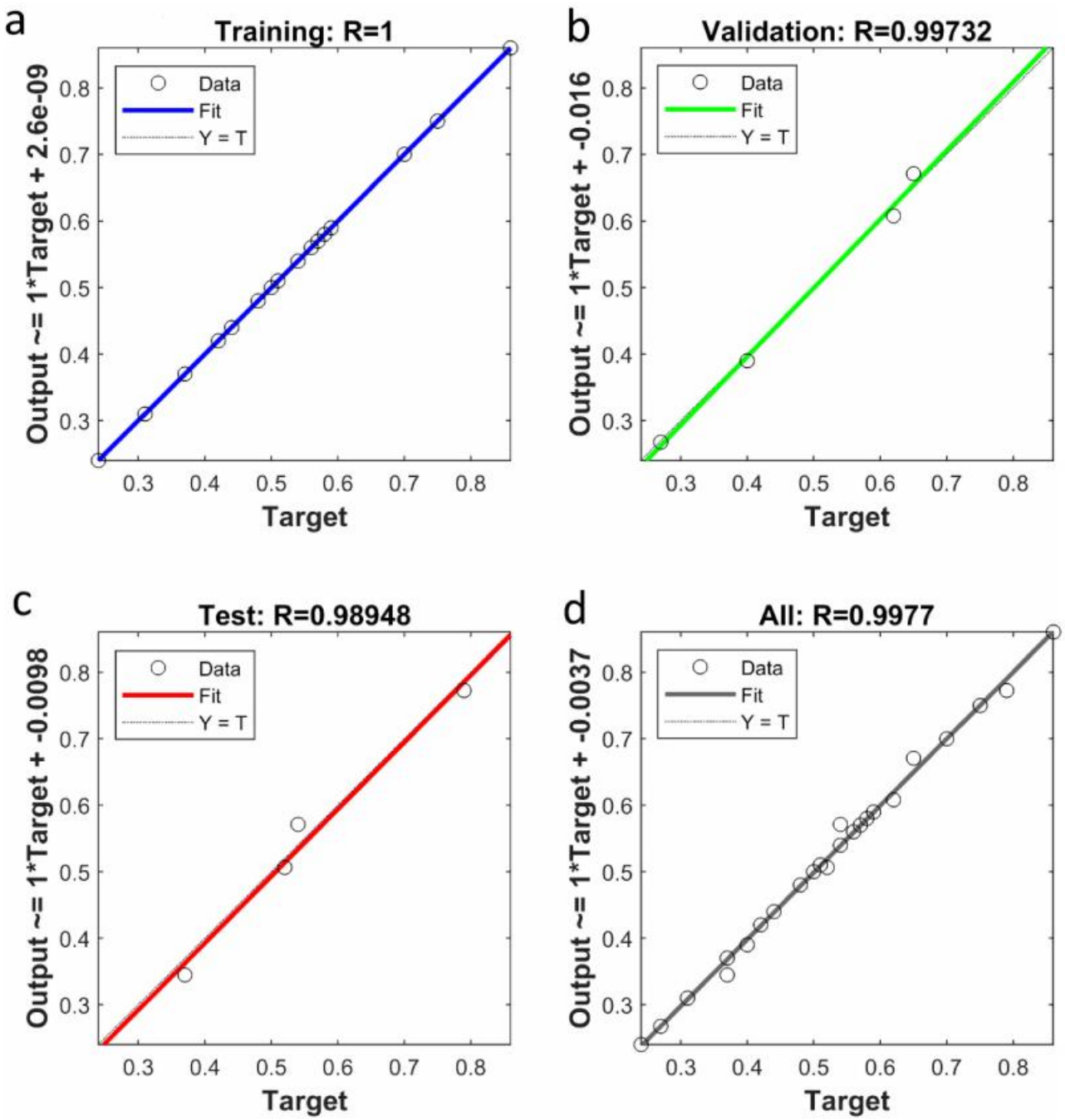

FIG. 8. HAZ width regression graphs: (a) Training dataset, (b) validation dataset, (c) test dataset, and (d) all dataset.

answers. Each individual of this set represents a response for the problem and evolves in each generation. All through each generation, chromosomes are evaluated by measuring the value of fitness. In order to form the next generation, two operators of crossover and mutation are used.

Table IV presents the considered parameters for optimization using the genetic algorithm. Based on Table II, the number of input and output variables is three and two in that order. The primary population for optimization is considered 40. In the genetic algorithm, it is necessary to create a set of possible solutions

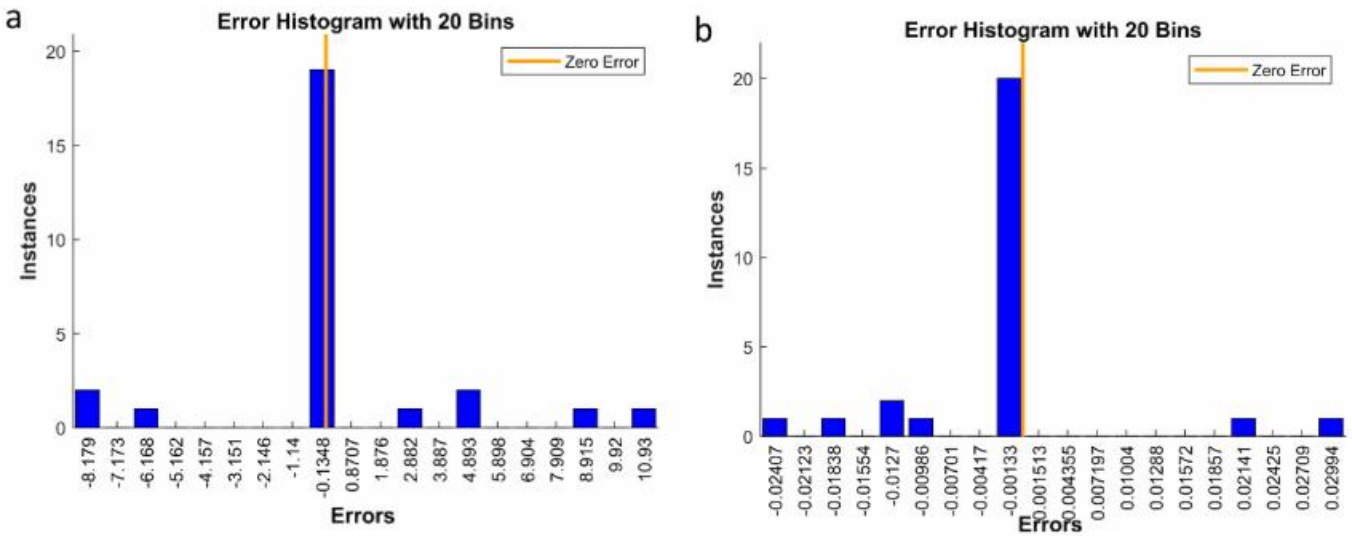

FIG. 9. Error histogram: (a) Maximum temperature and (b) HAZ width.

as the initial population as the first step. The mentioned set of solutions is selected randomly. How to crossover the parents of primary population is in the form of intermediate. As is shown in Eq. (7), a crossover along with the consideration of the average weight of the parents leads to the creation of children. Weights are determined by a single parameter (ratio) that is the scale of the number of variables. Crossover fraction determines the fraction of the next generation, which is produced by combination operation, and its value is equal to a fraction between zero and one. In the present study, the value of the crossover fraction is considered equal to 0.8. The mutation is an operation in which one or more genes in a selected chromosomal strand change from zero to one or *vice versa* creating mutant generation. In general, the mutation operator leads to the entrance of new information to the population and searching for intact spaces in the problem. The feasible adapt mutation is used in the present study, which results in a large increase in the population and thus an increase in algorithm efficiency in multiobjective optimization. The migration fraction is a criterion from zero to one which specifies a fraction of people in each subgroup migrating to different subgroups. The cessation provision

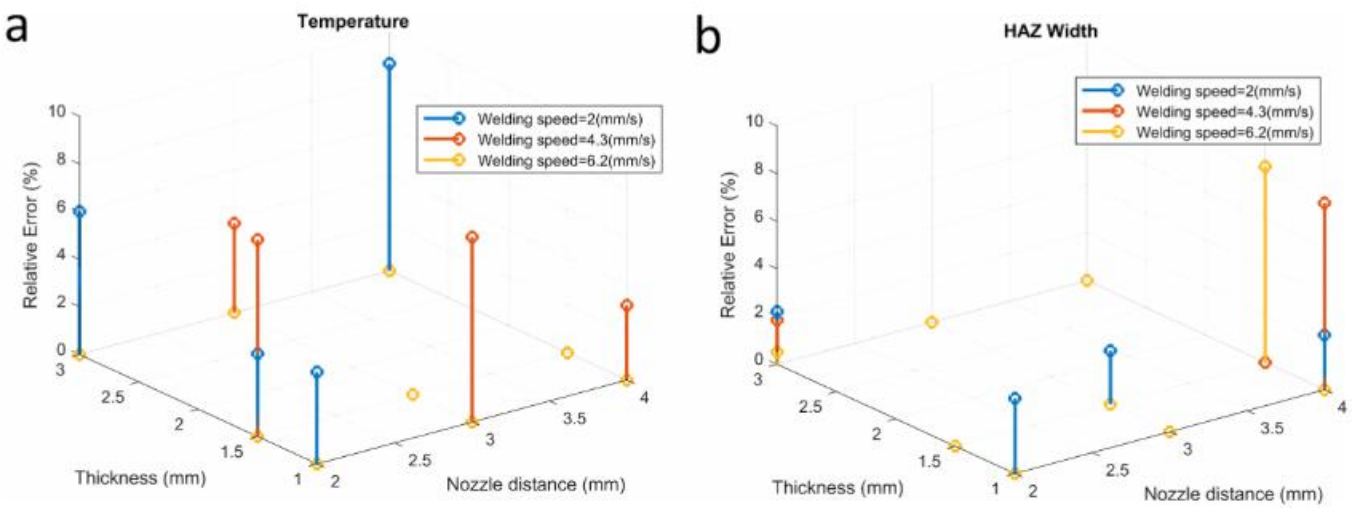

FIG. 10. The relative error for the input values: (a) Temperature and (b) HAZ width.

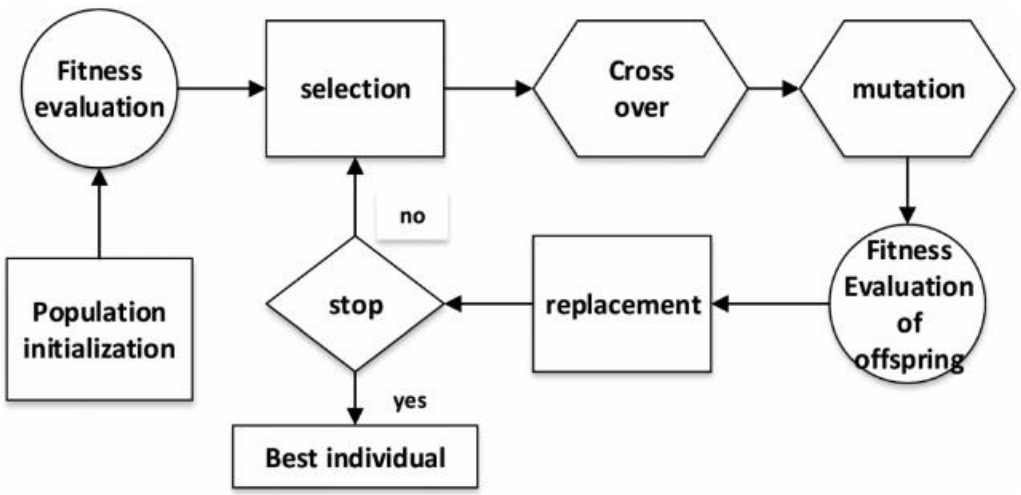

FIG. 11. The optimization procedure using the genetic algorithm (Ref. 35).

of generation production was considered, given the maximum time elapsed without improving the evolution,

$$child = parent\ 1 + r\,and^{*}Ratio^{*}(parent\ 2 - parent\ 1). \quad (7)$$

V. RESULTS AND DISCUSSION

Figures 12 and 13 indicate the ANN results for the temperature and HAZ width at 3 mm nozzle distance. As shown in Fig. 12, the thickness variations at low speeds have an impressive effect on temperature. It should be mentioned that in a constant speed, the lower thickness piece experiences higher temperature. This indicates that a thin piece acts as a small heat sink. The points identified by "*" indicate the data resulted from the experimental work.

As shown in Fig. 13, increasing welding speed causes declining energy absorption; so, this results in decreasing amount of melt and HAZ. Generally, HAZ can be decreased by increasing thickness and welding speed. Hence, it can be realized that welding speed and thickness have an incredible effect on microstructure, weld quality, and molten pool dimensions.

TABLE IV. Genetic algorithm parameters.

Parameter	Value
Inlet	3
Output	2
Population size	40
Generations	42
Crossover fraction	0.8
Crossover Fcn	Crossover intermediate
Mutation Fcn	Mutation adapt feasible
Migration fraction	0.2

In Fig. 14, the impression of the focal position change on HAZ width has been demonstrated in a constant welding speed of 3 *mm*/s. The power density alternates through the laser focus displacement. Therefore, identifying the optimal focus position significantly contributes to forming an excellent weld. The results of Fig. 14 represent that thickness reduction significantly increases the HAZ width dependence on the focal position. Furthermore, it was observed that at a specified thickness and 4 mm nozzle distance, where the laser focus is 1 mm below the workpiece surface, and the minimum HAZ width is obtained.

Figure 15 shows the variations of HAZ width at 1.5 mm thickness. It is observed that by locating the nozzle distance at the

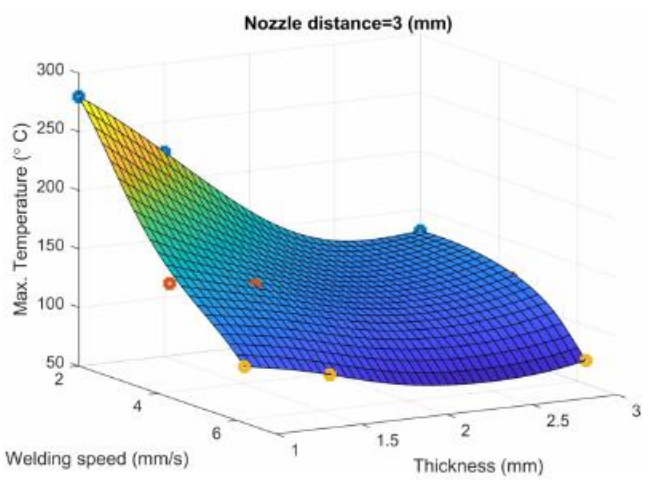

FIG. 12. The changes of maximum temperature in terms of thickness and welding speed at 3 mm nozzle distance.

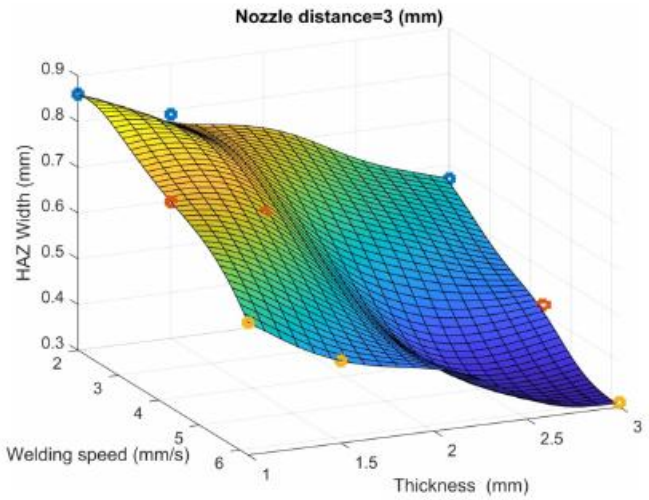

FIG. 13. The changes of HAZ width in terms of thickness and welding speed at 3 mm nozzle distance.

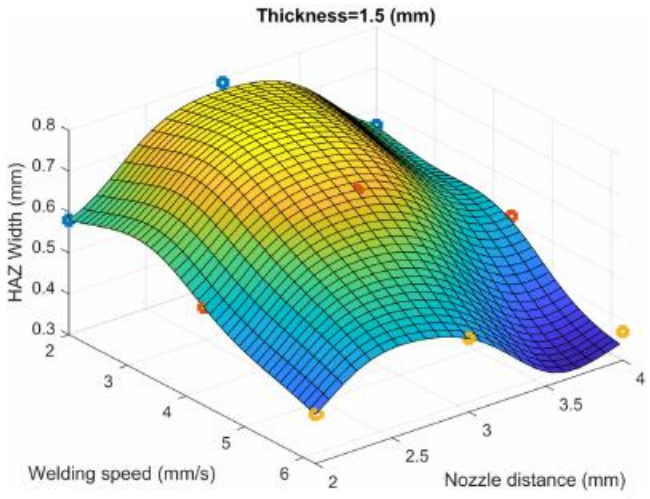

FIG. 15. The changes of HAZ width in terms of nozzle distance and welding speed at 1.5 mm thickness.

vicinity of the workpiece surface, the HAZ width increases due to increasing the temperature and melting workpiece surface. In order to improve the weld quality and reduce the HAZ width, one can increase the welding speed.

It is worthy to mention that the heat-affected zone leads to making residual stresses in the main structure of the workpiece and the weld zone. These stresses can result in harmful effects like the corrosion cracks and fatigue resistance reduction of the workpiece. Although heightening temperature increases the volume of melt, there will be a wider HAZ. Therefore, reducing the HAZ width can be important. The result of solution is just a response in single-objective optimization, but in the two-objective optimization, it is in the form of a set of responses known as pareto front. The set of pareto responses is the optimal response from the response space neither of which is better than the other. This being better is based on the criteria that are defined in the target functions and the constraints of multiobjective optimization problem. Figure 16 is an indication of ANN optimized output parameters including maximum temperature and HAZ. The optimized parameters for the welding

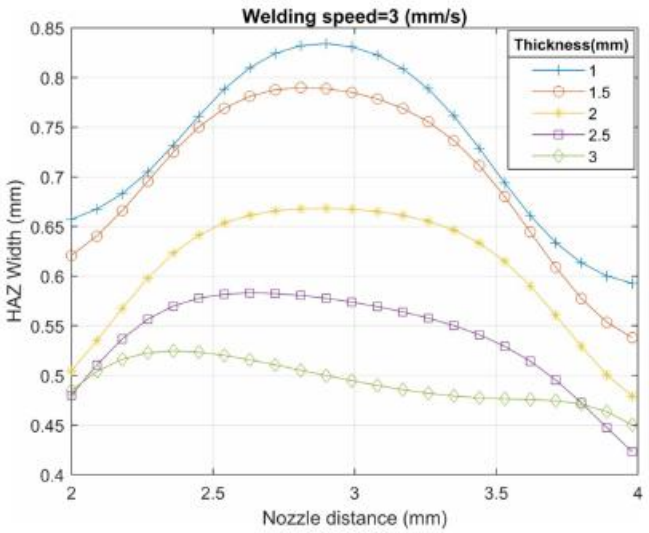

FIG. 14. The changes of HAZ width in terms of nozzle distance and thickness at 3 mm/s welding speed.

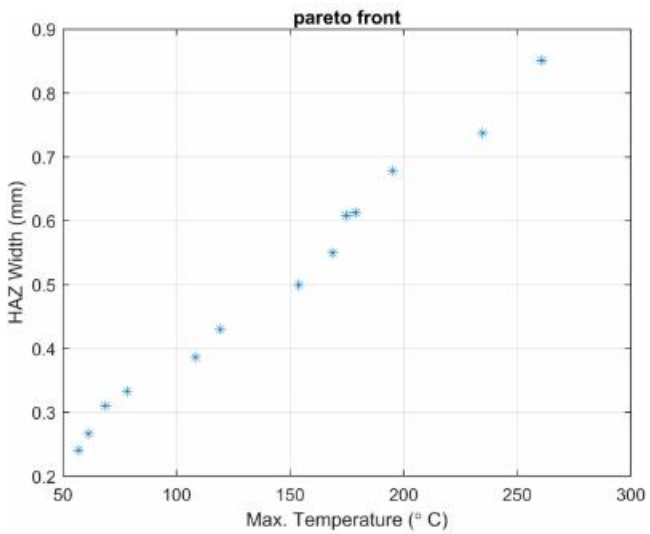

FIG. 16. The optimized output parameters of temperature and HAZ width.

TABLE V. Optimal input and output values.

Welding speed (mm/s)	Thickness (mm)	Nozzle distance (mm)	Max. temperature (°C)	HAZ width (mm)
6.185 710 095	2.812 170 046	3.988 997 061	56.959 305 81	0.240 884 09
2.042 206 291	1.759 227 398	2.880 670 148	195.215 303 2	0.678 426 124
2.209 782 042	2.094 858 068	3.107 970 298	153.815 658 9	0.499 658 858
5.774 845 896	2.238 001 652	3.508 186 649	68.731 607 77	0.310 049 191
2.034 926 664	1.016 873 974	2.634 938 299	260.805 475 6	0.850 788 546
4.716 162 229	2.735 592 135	3.844 930 447	78.207 300 52	0.333 137 775
2.134 782 359	1.829 820 172	3.124 545 218	178.762 664 4	0.612 461 967
5.989 374 81	2.672 185 587	3.551 362 972	61.207 798 25	0.266 658 703
4.909 030 618	2.462 362 466	3.069 118 112	108.358 676	0.386 012 138
2.284 926 664	1.016 873 974	2.134 938 299	234.712 281 2	0.737 443 162
2.729 868 695	2.481 097 297	3.483 318 355	119.125 946 2	0.429 883 836
2.191 832 849	1.838 105 354	3.116 314 531	174.769 407 9	0.608 352 353
2.042 206 291	1.759 227 398	2.880 670 148	195.215 303 2	0.678 426 124
2.032 311 333	2.026 401 319	2.948 589 015	168.688 094 8	0.549 376 349

speed, laser nozzle distance, and thickness were obtained in the interval of 2–6.2 mm/s, 2–4 mm, and 1–3 mm in that order.

Table V presents the input parameters including welding speed, nozzle distance, and thickness to achieve the optimal outputs. According to Table V, the minimum HAZ width is obtained by increasing the laser welding speed and the nozzle distance of laser penetration to the piece. Besides, at low thicknesses, the HAZ width can be substantially decreased by increasing the nozzle distance.

VI. CONCLUSION

In this study, an artificial neural network was used to predict the dimensions of HAZ and maximum temperature. Moreover, using the genetic algorithm, the parameters of optimal speed, nozzle distance, and thickness were obtained to reduce the HAZ width. The results of current research work are as follows:

- The results obtained in this study show the high capability of ANN in the estimation of laser welding parameters. The maximum relative error of ANN output data and real one for the HAZ width and maximum temperature were obtained to be 8.22% and 8.62%, respectively, which indicates the closeness of the predicted values to the experimental data.
- In this study, 12 ANN training algorithms were compared to each other and the Levenberg–Marquardt algorithm was chosen as the best one based on the mean square error. Furthermore, the lowest error for the HAZ width and temperature was related to the network with 11 and 8 neurons in the hidden layer, respectively. On the other hand, increasing the number of neurons does not necessarily result in improving training performance.
- The results demonstrated that for the identical conditions, the thickness reduction of the segment considerably increases the HAZ width. In contrast, the thicker plate underwent a higher temperature gradient in comparison to the thinner plate.
- The multiobjective genetic algorithm was employed in order to optimize the input parameters to achieve higher temperature and lower HAZ width. The optimization results showed that the HAZ width decreases by increasing the welding speed and thickness.

REFERENCES

[1]R. Wang, S. Xu, Y. Yue, and X. Wang, "Thermal behavior of materials in laser-assisted extreme manufacturing: Raman-based novel characterization," Int. J. Extreme Manuf. **2**, 032004 (2020).
[2]K. Cvecek, S. Dehmel, I. Miyamoto, and M. Schmidt, "A review on glass welding by ultra-short laser pulses," Int. J. Extreme Manuf. **1**, 042001 (2019).
[3]M. Kasuga, T. Sano, and A. Hirose, "Grain refining in weld metal using short-pulsed laser ablation during CW laser welding of 2024-T3 aluminum alloy," Int. J. Extreme Manuf. **1**, 045003 (2019).
[4]J. Xue, M. H. Razavi Dehkordi, A. Abdelahi, A. Abdelahi, E. Rasti, and Z. Li, "Experimental investigation of temperature field, defects, and mechanical strength in dissimilar laser bonding of Ti6Al4 V and polyethylene terephthalate," J. Laser Appl. **33**, 012038 (2021).
[5]G. S. Kumar, K. Raghukandan, S. Saravanan, and N. Sivagurumanikandan, "Optimization of parameters to attain higher tensile strength in pulsed Nd:YAG laser welded hastelloy C-276–monel 400 sheets," Infrared Phys. Technol. **100**, 1–10 (2019).
[6]G. Casalino, F. Curcio, and F. M. C. Minutolo, "Investigation on Ti6Al4 V laser welding using statistical and taguchi approaches," J. Mater. Process. Technol. **167**, 422–428 (2005).
[7]M. S. F. d. Lima, "Laser beam welding of titanium nitride coated titanium using pulse-shaping," Mater. Res. **8**, 323–328 (2005).
[8]J. R. Berretta, W. de Rossi, M. D. M. das Neves, I. A. de Almeida, and N. D. V. Junior, "Pulsed Nd:YAG laser welding of AISI 304 to AISI 420 stainless steels," Opt. Lasers Eng. **45**, 960–966 (2007).
[9]X. Cao and M. Jahazi, "Effect of welding speed on butt joint quality of Ti–6Al–4 V alloy welded using a high-power Nd:YAG laser," Opt. Lasers Eng. **47**, 1231–1241 (2009).
[10]E. Taban, E. Deleu, A. Dhooge, and E. Kaluc, "Laser welding of modified 12% Cr stainless steel: Strength, fatigue, toughness, microstructure and corrosion properties," Mater. Des. **30**, 1193–1200 (2009).
[11]A. P. L. Aleksander, "Laser welding of titanium alloy Ti6Al4 V using a disk laser," MTM J. **7**, 53–56 (2012).
[12]M. Torkamany, F. M. Ghaini, and R. Poursalehi, "Dissimilar pulsed Nd:YAG laser welding of pure niobium to Ti–6Al–4 V," Mater. Des. **53**, 915–920 (2014).

[13]F. Caiazzo, V. Alfieri, I. Fierro, and V. Sergi, "Investigation and optimization of disk-laser welding of 1 mm thick Ti-6Al-4V titanium alloy sheets," Adv. Mech. Eng. **7**, 373561 (2015).
[14]S. L. Campanelli, G. Casalino, M. Mortello, A. Angelastro, and A. D. Ludovico, "Microstructural characteristics and mechanical properties of Ti6Al4 V alloy fiber laser welds," Procedia CIRP **33**, 428–433 (2015).
[15]J. Ahn, L. Chen, C. Davies, and J. Dear, "Parametric optimisation and microstructural analysis on high power Yb-fibre laser welding of Ti–6Al–4 V," Opt. Lasers Eng. **86**, 156–171 (2016).
[16]R. Palanivel, I. Dinaharan, and R. Laubscher, "A comparative study on microstructure and mechanical properties between friction and laser beam welded titanium tubes," Optik **177**, 102–111 (2019).
[17]Y. Ai, P. Jiang, C. Wang, G. Mi, and S. Geng, "Experimental and numerical analysis of molten pool and keyhole profile during high-power deep-penetration laser welding," Int. J. Heat Mass Transfer **126**, 779–789 (2018).
[18]P. Kumar and A. N. Sinha, "Effect of heat input in pulsed Nd:YAG laser welding of titanium alloy (Ti6Al4V) on microstructure and mechanical properties," Weld. World **63**, 673–689 (2019).
[19]M. Raja Kumar, J. Jouvard, I. Tomashchuk, and P. Sallamand, "Vapor plume and melted zone behavior during dissimilar laser welding of titanium to aluminum alloy," Proc. Inst. Mech. Eng. Part L **234**, 681–696 (2020).
[20]K. Benyounis, A. Olabi, and M. Hashmi, "Effect of laser welding parameters on the heat input and weld-bead profile," J. Mater. Process. Technol. **164**, 978–985 (2005).
[21]W.-S. Chang and S.-J. Na, "Prediction of laser-spot-weld shape by numerical analysis and neural network," Metall. Mater. Trans. B **32**, 723–731 (2001).
[22]E. Anawa and A.-G. Olabi, "Optimization of tensile strength of ferritic/austenitic laser-welded components," Opt. Lasers Eng. **46**, 571–577 (2008).
[23]Y. W. Park and S. Rhee, "Process modeling and parameter optimization using neural network and genetic algorithms for aluminum laser welding automation," Int. J. Adv. Manuf. Technol. **37**, 1014–1021 (2008).
[24]P. Sathiya, K. Panneerselvam, and M. A. Jaleel, "Optimization of laser welding process parameters for super austenitic stainless steel using artificial neural networks and genetic algorithm," Mater. Des. **36**, 490–498 (2012).
[25]M. I. S. Ismail, Y. Okamoto, and A. Okada, "Neural network modeling for prediction of weld bead geometry in laser microwelding," Adv. Opt. Technol. **2013**, 1–7.
[26]M. Akbari, S. Saedodin, A. Panjehpour, M. Hassani, M. Afrand, and M. J. Torkamany, "Numerical simulation and designing artificial neural network for estimating melt pool geometry and temperature distribution in laser welding of Ti6Al4 V alloy," Optik **127**, 11161–11172 (2016).
[27]A. Bagchi, S. Saravanan, G. S. Kumar, G. Murugan, and K. Raghukandan, "Numerical simulation and optimization in pulsed Nd:YAG laser welding of hastelloy C-276 through Taguchi method and artificial neural network," Optik **146**, 80–89 (2017).
[28]T. D. B. Kannan, T. Ramesh, and P. Sathiya, "Application of artificial neural network modelling for optimization of Yb:YAG laser welding of nitinol," Trans. Indian Inst. Met. **70**, 1763–1771 (2017).
[29]N. Sivagurumanikandan, S. Saravanan, G. S. Kumar, S. Raju, and K. Raghukandan, "Prediction and optimization of process parameters to enhance the tensile strength of Nd:YAG laser welded super duplex stainless steel," Optik **157**, 833–840 (2018).
[30]M. Mehrpouya, A. Gisario, H. Huang, A. Rahimzadeh, and M. Elahinia, "Numerical study for prediction of optimum operational parameters in laser welding of NiTi alloy," Opt. Laser Technol. **118**, 159–169 (2019).
[31]B. Liu, W. Jin, A. Lu, K. Liu, C. Wang, and G. Mi, "Optimal design for dual laser beam butt welding process parameter using artificial neural networks and genetic algorithm for SUS316L austenitic stainless steel," Opt. Laser Technol. **125**, 106027 (2020).
[32]Z. Li, K. Rostam, A. Panjehpour, M. Akbari, A. Karimipour, and S. Rostami, "Experimental and numerical study of temperature field and molten pool dimensions in dissimilar thickness laser welding of Ti6Al4 V alloy," J. Manuf. Processes **49**, 438–446 (2020).
[33]H. Demuth and M. Beale, *Neural Network Toolbox User's Guide For Use with MATLAB®* (The MathWorks Inc., Natick, MA, 2002).
[34]M. T. Hagan and M. B. Menhaj, "Training feedforward networks with the Marquardt algorithm," IEEE Trans. Neural Networks **5**, 989–993 (1994).
[35]T. Murata and H. Ishibuchi, "MOGA: Multi-objective genetic algorithms," in *IEEE International Conference on Evolutionary Computation* (IEEE, Perth, Australia, 1995).